INTERNATIONAL JOURNAL OF AUTOMOTIVE AND MECHANICAL ENGINEERING
ISSN: 2229-8649 e-ISSN: 2180-1606
VOLUME 22, ISSUE 3, 2025, 12788 - 12800
DOI: https://doi.org/10.15282/ijame.22.3.2025.18.0975

RESEARCH ARTICLE

Wheel–Road Separation Phenomenon in the Frequency Response of a Half–Car Model

Nguyen Dang Quy[1], Nguyen Truong Sinh[1]*, Vu Ngoc Tuan[1], To Viet Thanh[1], Vu Manh Dung[1], Tran Cong Thuc[2], Pham The Hung[2], and Reza Jazar[3]

[1]Institute of Vehicle and Energy Engineering, Le Quy Don Technical University, 100000 Hanoi, Vietnam
[2] Faculty of Technology and Engineering, Thai Binh University, 06000 Thai Binh, Vietnam
[3]College of Engineering, Tarleton State University, Stephenville, TX, USA

ABSTRACT – The paper presents the vibration dynamics of a half–car system in the frequency domain, taking into account the tyre–road separation. It focuses on how the car changes between two states: when the tyres are in contact with the road and when they lose contact. The vibration equations were developed to incorporate this change using a special condition known as the "separation condition." This condition was applied to both left and right wheels using indicator functions, which allows for observing the actual frequency response, including the vertical and roll dynamics. The study also examined how different road surfaces and car designs impact the car's motion when tyre separation occurs. The simulation results show that this new model is 16% more accurate than older models when the mass centre is far from the middle. Overall, the research offers valuable insights for designing more effective suspension systems and refining control strategies to prevent rollovers and maintain vehicle stability.

ARTICLE HISTORY
Received : 08th Oct. 2024
Revised : 05th June 2025
Accepted : 29th July 2025
Published : 30th Sept. 2025

KEYWORDS
Vehicle vibrations
Tyre–road separation
Half–car vibrations
Roll dynamics
Vehicle stability
Frequency response

1. INTRODUCTION

Vibration dynamics is an important factor, as it affects ride comfort and passenger safety, especially in cases of wheel–road separation. In terms of vehicle dynamics, it is generally assumed that all wheels touch the ground [1–3]. However, in realistic situations, the wheels may separate from the road. The tyre–road separation may occur at high amplitudes and high frequencies of road excitation, or when the vehicle travels at high speeds [4]. The tyre–road separation phenomenon creates a space between the tyres and the surface profile [5]. In a vehicle ride, tyre–road separation occurs if the tyres briefly lose contact with the ground, and the vehicle only makes contact with the surface again due to gravitational force [6]. Furthermore, the tyre–road contact model has a significant influence on the dynamic forces transmitted by the tyre. Therefore, the separation dynamics reduce the maintenance of traction, handling, ride quality, and rollover potential when the vehicle is in motion [8–9]. During separation time, the tyre cannot provide the necessary traction and grip, which can briefly affect how the vehicle handles until contact is restored. This separation can cause a jolt or sudden change in motion, reducing ride comfort [4]. The sudden loss and regain of contact can send vibrations and shocks to passengers [10]. The contact characteristics between the tyre and the road have a significant impact on the stress distribution [11], which in turn generates friction forces. The space between the wheel and the ground is essential for braking, accelerating, and turning. Temporary separation can break these processes, affecting the car's safety [12]. Thus, investigating the vibrating system is important to know how the separation phenomena affect ride comfort as well as safety.

Currently, few studies have observed the wheel–road separation phenomenon in simple models [13, 14]. A simple bicycle–car model has been used to investigate tyre–road separation, considering the impact of the mass ratio [15]. A four–degree–of–freedom (DOF) bicycle–car model can be complicated to investigate and optimize the piecewise dynamic system [16]. Although numerous studies on active and semi–active suspension systems have been published in recent decades, the issue of tyre–road separation has not received significant attention in recent years [17]. The half–car model with 4 degrees of freedom can be chosen for the analysis, as it offers a balanced trade–off between model complexity and insight into suspension performance [18]. These automotive studies focus on designing vehicles with active suspension systems to reduce vertical amplitude and acceleration, thereby improving ride comfort under normal driving conditions. Meanwhile, these vehicle models do not exhibit roll motion. Furthermore, among the numerous causes of vehicle accidents, rollovers require special attention. When a vehicle rollover occurs, it not only reduces comfort but can also lead to tragic accidents [19, 20].

To analyse the dynamics of roll in a vibrating system, a full–car model should be introduced. However, the full–car vibrating model has a high degree of freedom and becomes more complex with the separation assumption. Moreover, a quarter–car model cannot capture roll motion, as it only accounts for vertical displacements. In contrast, the half–car model provides more accurate predictions of dynamic response and has greater potential for real–world applications. To enhance ride comfort and handling performance, an optimal control method can be developed using a half–car roll model [21]. A half–car model related to roll dynamics, considering tyre–road separation, has never been studied. Analysis of the

*CORRESPONDING AUTHOR | Nguyen Truong Sinh | ✉ sinh.nguyentruong@lqdtu.edu.vn

vibrating frequency in this model is important, as it provides valuable insight into roll dynamics, which remarkably affects vehicle stability during travel. Moreover, the safety of a moving vehicle depends on stability performance [22]. Consequently, this paper focuses on examining how road conditions and the location of the car's mass centre influence roll as well as vertical responses. This is the first study to model tyre–road separation in the frequency domain using a 4–DOF half-car model, with indicator–based switching between in–contact and no–contact states.

The study will be presented as follows: The half–car vibration model is introduced in Section 2, covering the governing equations, separation conditions, and the concept of frequency characteristics. Section 3 presents the simulation results for both vertical and roll responses under the assumptions of separation and no-separation. The conclusions summarise the key findings.

2. VEHICLE MODELLING

In the section, a half–car model is presented along with its corresponding differential equations in the dimensional field. Furthermore, the concept of the frequency domain of tyre–road separation is explored.

2.1 Model and Governing Equation System

To analyse and optimise vehicle roll dynamics, a half–car vibrating model could be utilised [1]. Figure 1 schematically depicts the wheel–road separation model for reference. The model is viewed from the front, taking into account the effect of an anti–roll bar that connects the two wheels to the car body [1]. This model considers the vertical displacement of the car body x, the displacements of the left and right tyres x_1, x_2, roll angle φ, and independent excitation profiles x_{r1} and x_{r2}. To simplify the analysis, the half–car system is modelled as a solid structure composed of three rigid boxes. A rigid box representing the car body is presented, with a mass of m. The bar has an inertia moment of I_x and represents the front mass of the vehicle body, it can be calculated using the inertia equation for a bar with a length of l. The m_1, m_2 are mass of two wheels and the tyre are often assumed equal in typical vehicle designs. The stiffness of the tyre is represented by k_t. Since the damping value of the tyre is significantly smaller compared to the main damper in the suspension system, the simulation can neglect the damper of tyres for a convenient study of wheel–road separation. The car's suspension system features a damping coefficient, c and a stiffness coefficient, k. The car is typically designed with symmetrical right and left suspensions, meaning that the stiffness coefficients and damping coefficients for both sides are equal.

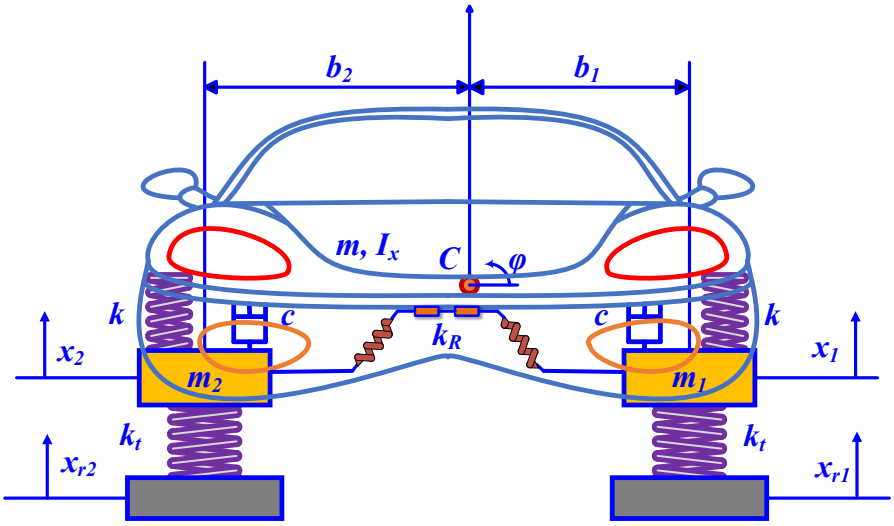

Figure 1. Modelling of half–car suspension system

In the contact state, the vibration dynamics follow the equations shown below [1]:

$$m\ddot{x} + c(\dot{x} - \dot{x}_1 + b_1\dot{\varphi}) + c(\dot{x} - \dot{x}_2 - b_2\dot{\varphi}) + k(x - x_1 + b_1\varphi) + k(x - x_2 - b_2\varphi) = 0 \quad (1)$$

$$I_x\ddot{\varphi} + b_1c(\dot{x} - \dot{x}_1 + b_1\dot{\varphi}) - b_2c(\dot{x} - \dot{x}_2 - b_2\dot{\varphi}) + b_1k(x - x_1 + b_1\varphi) - b_2k(x - x_2 - b_2\varphi) + k_R\varphi = 0 \quad (2)$$

$$m_1\ddot{x}_1 - c(\dot{x} - \dot{x}_1 + b_1\dot{\varphi}) + k_t(x_1 - x_{r1}) - k(x - x_1 + b_1\varphi) = 0 \quad (3)$$

$$m_2\ddot{x}_2 - c(\dot{x} - \dot{x}_2 - b_2\dot{\varphi}) + k_t(x_2 - x_{r2}) - k(x - x_2 - b_2\varphi) = 0 \quad (4)$$

when the tyres do not touch the ground at a large bump or high speeds, the body bounce and roll still follow equations (1) and (2), while the motion equations of the two wheels will be:

$$m_1\ddot{x}_1 - c(\dot{x} - \dot{x}_1 + b_1\dot{\varphi}) - k(x - x_1 + b_1\varphi) + (m_1 + \frac{b_2}{b}m)g = 0 \tag{5}$$

$$m_2\ddot{x}_2 - c(\dot{x} - \dot{x}_2 - b_2\dot{\varphi}) - k(x - x_2 - b_2\varphi) + (m_2 + m\frac{b_1}{b})g = 0 \tag{6}$$

These two equations (5) and (6) in the no–contact state are novel and have never been published in any previous papers. The model described above will be investigated in both separation and non-separation situations corresponding to the two equation systems. This system will examine the transitions between the contact and no–contact states of the tyre and road under harmonically bumpy roads. The half–car vibration model is excited by the rough surfaces. The amplitude of the roadway is represented by y_0 and ω denotes the angular frequency. The road profiles are mathematically defined as: $x_{r1} = y_0 sin\omega t$; $x_{r2} = y_0 sin\omega t$.

2.2 Separation Condition

When the tyre experiences a vertical bounce that is less than the tyre's static compression, the tyre still touches the ground. Conversely, if the tyre moves a gap greater than the tyre's static compression, it will lose contact and enter a state of free flight. In this study, to analyse the separation process, the tyre–road separation condition can be measured by the tyre's static compression. This separation condition applies to different cases where either the left wheel or the right tyre is separated, or when both tyres are separated simultaneously. The discontinuous differential equation system of a half–car model will be solved using the separation condition and a numerical strategy. Numerical integration is used to study how vehicles vibrate when going over a road bump, looking for possible tyre–road separation. This study employs MATLAB's ode45 solver to perform the necessary numerical calculations related to the separation condition.

In–contact condition for left wheel: $x_1 - x_{r1} < x_{T1}$ (7)

No–contact condition for left wheel: $x_1 - x_{r1} \geq x_{T1}$ (8)

In–contact condition for right wheel: $x_2 - x_{r2} < x_{T2}$ (9)

No–contact condition for right wheel: $x_2 - x_{r2} \geq x_{T2}$ (10)

where, $x_{T1} = \dfrac{(m_1 + m\frac{b_2}{b})g}{k_t}$ and $x_{T2} = \dfrac{(m_2 + m\frac{b_1}{b})g}{k_t}$ are static compression.

To detect the loss of tyre–road contact, two indicator functions, I_1, I_2, are utilised for the corresponding wheels. Let us define the indicator as Heaviside functions to identify tyre–road separation during the vehicle's motion.

$$I_1 = Heaviside(x_1 - x_{r1} - x_{T1}) = \begin{cases} 0.05 & x_1 - x_{r1} \geq x_{T1} \\ 0 & x_1 - x_{r1} < x_{T1} \end{cases} \tag{11}$$

$$I_2 = Heaviside(x_2 - x_{r2} - x_{T2}) = \begin{cases} -0.05 & x_2 - x_{r2} \geq x_{T2} \\ 0 & x_2 - x_{r2} < x_{T2} \end{cases} \tag{12}$$

There are two indicator functions I_1, I_2, that will switch the system of differential equations for vibrating motion from (1), (2), (3), and (4) to (1), (2), (5), and (6), depending on different scenarios, including whether the tyres touch the rough surfaces or not. The indicator shows that separation occurs when its value is not equal to zero. In the half–car model, the two positive indicators correspond to the right and left wheels, respectively.

2.3 Frequency Domain

The frequency domain represents how a system responds to various input frequencies, illustrating the relationship between the resulting amplitudes and the input frequencies [23]. For linear systems, the frequency response can be derived from time response solutions using methods like operational transformations to obtain analytical results [4]. Moreover, the frequency domain is more useful for assessing a system's sensitivity to noise and parameter variations [24–26]. Nevertheless, we do not have any exact strategies to identify the frequency domain of a complicated system [4]. This study employs perturbation techniques, which can provide an approximate frequency response for systems exhibiting weak nonlinearity.

3. RESULTS AND DISCUSSION

To obtain the vibration dynamic response considering the tyre–road assumption, let us examine a half–car system with the data provided in Table 1 [1]. To create a realistic model, the half–car model includes an anti–roll bar, which has a stiffness coefficient k_R.

When some damping is incorporated into a suspension, the suspension will technically reach a steady state in response to a harmonic input. Therefore, the steady-state amplitude can be obtained when the time is long enough, and the frequency response can be determined. For this reason, the research starts by using two harmonic excitations to investigate the half–car's time response. According to the data from Table 1 [1], the response appears to reach a steady state within 0.3 seconds. To ensure all time responses are in steady state, the amplitude is captured in the second half of the simulation interval. Capturing the amplitude for different frequencies from these responses will likely provide a good approximation of the frequency response.

Table 1. Data of half–car vibrating system

Parameters	Values	Parameters	Values
m	420 kg	I_x	820 kgm^2
m_1	53 kg	m_2	53 kg
b_1	0.7 m	b_2	0.75 m
k	10000 N/m	k_t	200000 N/m
c	1000 Ns/m	k_R	25000 N/m

Time response is important in vibrating systems because it helps to evaluate how the system behaves over time when subjected to an input. Thus, the time response for the in–contact state is simulated in Figure 2, with the same road excitation applied to both tyres. In this case, the tyres are always in contact with the ground due to a low road amplitude $y_0 = 0.01\ m$ and a low input frequency $\omega = 8\ rad/s$. Ignoring the transient period, the body and tyre bounces appear to vibrate harmonically, following the road excitation function. Here, the amplitude of the two–wheel response is approximately 0.01 m, while the amplitude of the body is approximately 0.015 m. It is noted that the displacement of the left wheel x_1 is consistent with the right wheel x_2 as the mass centre has been located nearly in the middle. Therefore, the roll angle is extremely small and may be negligible.

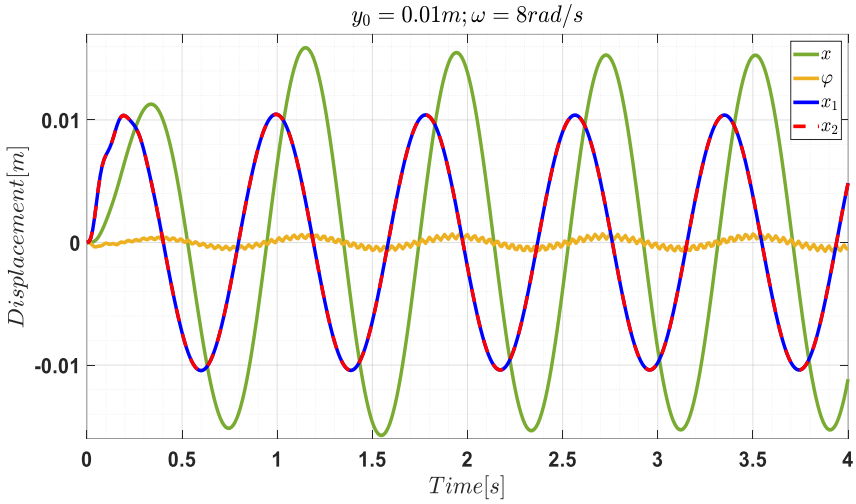

Figure 2. Time responses with the same amplitude of road excitation

Keeping the given input data, let us change the amplitude of the road excitation for the right wheel to $y_{02} = 0.02\ m$, both tyres are still in touch with the ground. The vibration dynamics of the model, shown in Figure 3, indicate that the hop of the right wheel x_2 fluctuates with a higher amplitude than the left one x_1. In detail, the amplitude of the left wheel response is approximately 0.01 m, while the amplitude of the right wheel response is approximately 0.02 m. Consequently, the maximum roll angle reaches 0.005 rad and increases significantly compared to that in Figure 2, indicating that the road inputs influence the roll response and increase when the road excitations differ between the two wheels. Therefore, roadways should be constructed without perturbations to avoid unexpected rollovers.

To clearly observe the tyres starting to leave the road surface, Figure 4 depicts the series of time responses during a separation scenario characterised by high amplitude and frequency of road excitation, $y_0 = 0.1\ m$, $\omega = 20\ rad/s$. The series comprises three planes: planes 1 and 2 display the displacements and separation indicators for the two corresponding wheels, whilst plane 3 demonstrates the body and roll motions. The wheel on the left-hand side begins to separate from the ground when the indicator function, I_1 reaches 0.05, which is a non-dimensional parameter represented by a logical value. Conversely, the wheel will return to the pavement if the value of I_1 drops to 0. The process occurs similarly for the right wheel in plane 2, with the limitation of the indicator, I_2 is –0.05. Therefore, the body angle is chaotic

as demonstrated in plane 3. The time response, considering the tyre–road separation, differs significantly from previous studies and is closer to real–world situations. Furthermore, the actual vibrating response, as shown by disturbed vibrations, negatively affects ride comfort for passengers. To minimise the body roll response, the vehicle should be designed using innovative strategies to delay the separation phenomenon that occurs in both wheels.

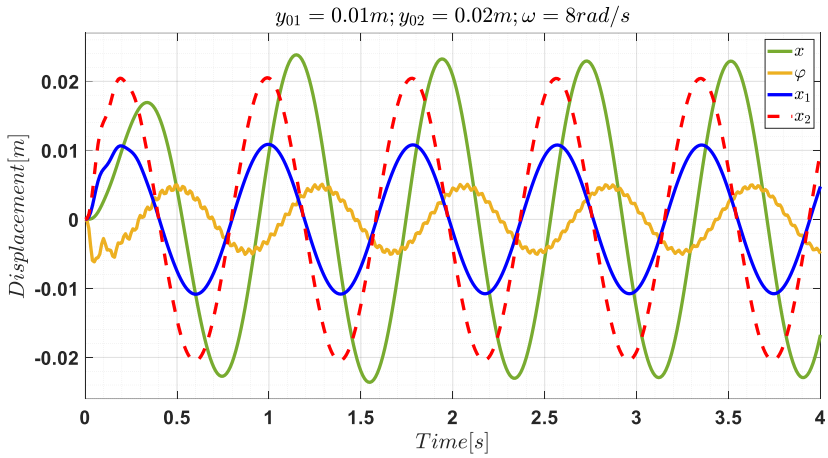

Figure 3. Time responses with different amplitudes of road excitation

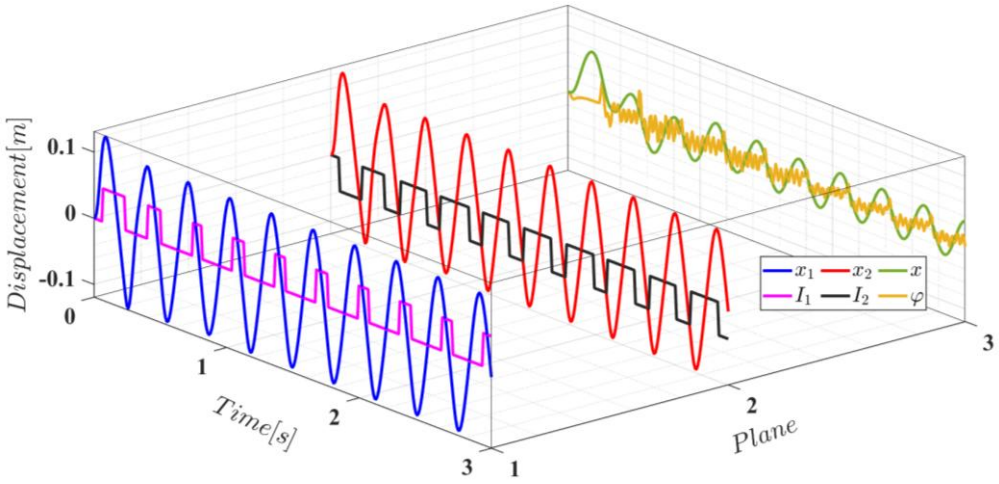

Figure 4. Series of time responses in no–contact state

A phase portrait serves a similar role to the frequency response, as it allows us to obtain both displacement and velocity values at each point of the interval, and it could also establish a relationship between velocity and acceleration. Thus, Phase plane analysis is a commonly used technique for studying nonlinear systems. It involves plotting trajectories on a two-dimensional graph that represents the system's behaviour using two state variables, showing how the system evolves under different initial conditions. This work will present the phase portraits of vertical responses, including the displacement and velocity of body bounce, roll motions, and two–wheel hop.

For the given suspension data in Table 1, Figure 5 plots phase portraits of both wheels under high amplitude and input frequency, $y_0 = 0.1\ m$, $\omega = 30\ rad/s$. These graphs show the relationship between the displacements and velocities of both wheels, as illustrated in Figures 5(a) and 5(b). The vertical displacement corresponding to the vertical velocity at each point in time for both tyres is represented by two lines parallel to the x_1 (x_2) and $\dot{x}_1$ ($\dot{x}_2$) axes. For the no–contact case, Figures 5(c) and 5(d) display three axes—vertical velocity, displacement, and time—forming a 3D helical shape, which corresponds to the 2D ellipse seen in Figures 5(a) and 5(b). Here, the 3D graphs are projected onto a 2D plane. However, the separation response deviates from this elliptical pattern. It is important to note that Figures 5a and 5b exclude the first period of the interval, while the other curves are plotted from the initial stage. Therefore, there is no disturbed vibration in Figures 5(a) and 5(b), and the initial responses are ignored.

Another view of the phase portrait is presented in Figure 6, which illustrates the relationship between the car's displacement and velocity for both body and roll motions. Both exhibit harmonic behaviour, forming an ellipse when projected onto a plane, as shown in Figures 6(a) and 6(b). However, when separation happens, the body bounce and roll response becomes more chaotic, as seen in Figures 6(c) and 6(d), significantly affecting passenger ride comfort. It is noted that the relationship between φ and $\dot{\varphi}$ in Figure 6(b), forms an ellipse because it is projected from the 3D graph in Figure 6(d) over a sufficiently long time period, 90 seconds. However, Figure 6(d) only shows the response over a short time

interval for clarity. Based on Figures 5 and 6, the simulation results obtained using the proposed approach do not exhibit a harmonic response, but rather resemble the actual dynamic behaviour more closely.

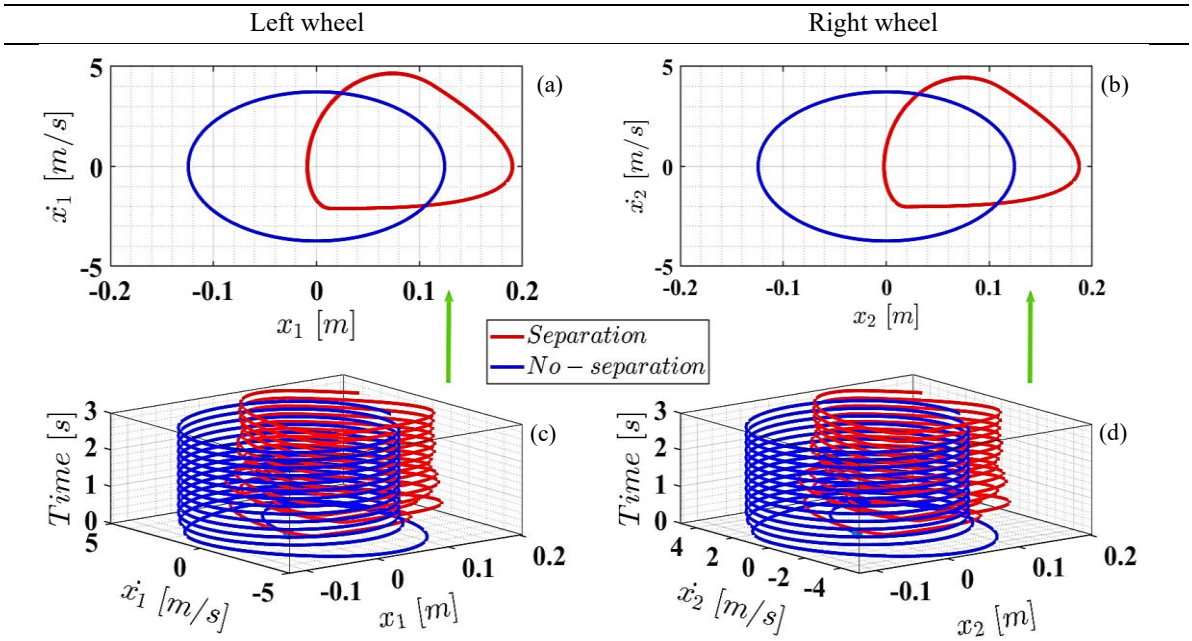

Figure 5. Phase portraits of two tyres

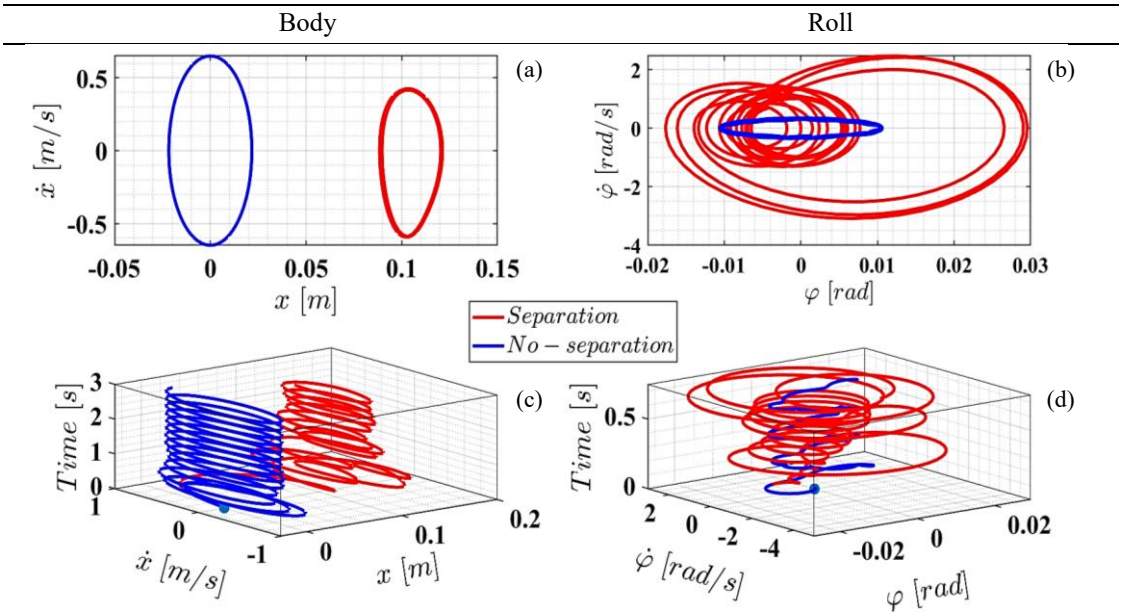

Figure 6. Phase portraits of body and roll motions

To understand dynamic responses across a wide range of input data, the frequency domain needs to be investigated. The determination of the body amplitudes, roll, and two wheels in the steady state can be performed using analytical solutions. Figure 7 illustrates the frequency domain of a non–dimensional field with two resonant frequencies, approximately $\omega_{01} = 6\ rad/s$, $\omega_{02} = 60\ rad/s$, which corresponds to the two natural frequencies. The purpose of the subplot is to guide drivers in avoiding resonant areas where the amplitudes of the vehicle body and tyres are incredibly high. The frequency response of two wheels and roll has the same shape, while the body's displacement is suddenly high at the first resonant frequency. Here, the resonance will cause the vehicle body to extend to twice the road input amplitude y_0, whereas the two wheels will extend to three times the road input amplitude y_0.

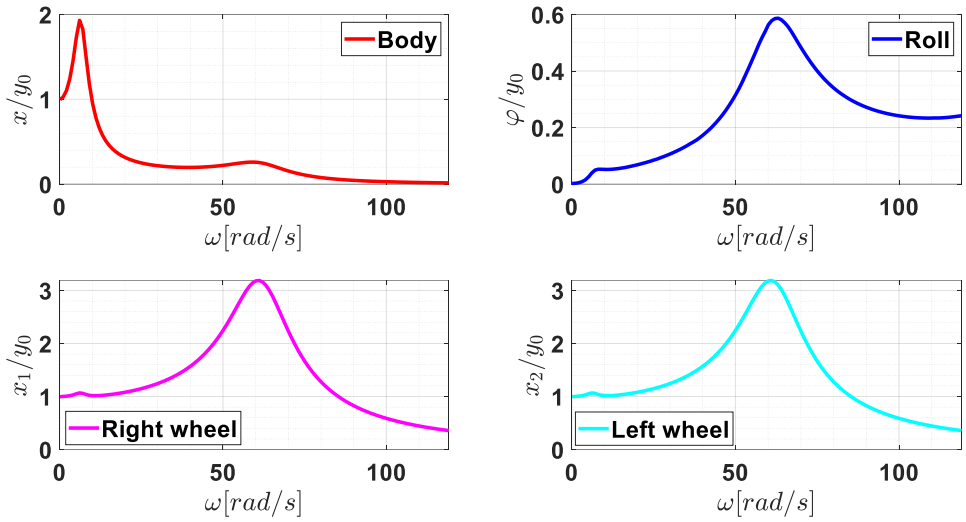

Figure 7. Frequency domain of a half–car model for the in–contact assumption

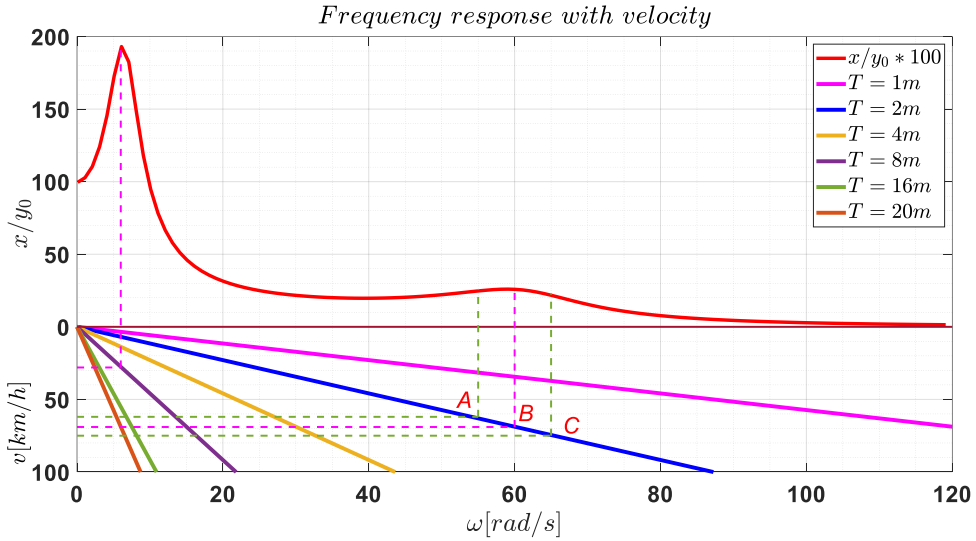

Figure 8. Identification of vehicle velocity to avoid resonance based on frequency response

The frequency response is not only important in determining resonant areas but also guides the driver in choosing an optimal longitudinal velocity for the vehicle, thereby enhancing ride comfort. Figure 8 depicts a graph with one horizontal axis for input frequency and two vertical axes: one for the ratio of the amplitude of body bounce to road displacement x/y_0, and the other for vehicle velocity v. It must be emphasised that the frequency response of the body comes from Figure 7, with the scale increased by 100 times to make the curve the same size as the velocity graph. The car's longitudinal velocity depends on the frequency ω and the period of time T of road excitation as explained below:

$$v = \frac{3.6T\omega}{2\pi} \left[\frac{km}{h}\right] \tag{13}$$

$$T = \{1\ 2\ 4\ 6\ 8\ 16\ 20\}[m] \tag{14}$$

The wavelength of the road surface profile is the distance between two points on the road where the profile repeats similarly, and it is typically used to assess the surface's roughness. The short wavelength range of the ground is from 0.5 to 1 m, the medium wavelength range is from 1 to 10 m, while the long wavelength range is greater than 10 m. Therefore, the study uses a road wavelength ranging from 1 to 20 m, as demonstrated in equation (14). There are six linear lines illustrating the relationship between vehicle velocity and input frequency of the road, corresponding to the six values of road wavelength in the matrix T. Each line provides a value of vehicle velocity at the resonant frequency; for instance, the line for $T = 8\ m$ identifies a longitudinal velocity of $v = 28\ km/h$ at the first resonant frequency $\omega_{01} = 6\ rad/s$. Similarly, the line for $T = 2\ m$ identifies a longitudinal velocity of $v = 69\ km/h$ at the second resonant frequency $\omega_{02} = 60\ rad/s$ as indicated by point B. By analysing the resonant characteristics, the line provides a range of vehicle velocities that reduce ride discomfort. If the vehicle travels on the road at a speed slower than 62 km/h at point A or faster than 75 km/h at point C, the resonance will be negligible for a road with a wavelength of 8 m.

The continuous tasks might use the analytic method to measure over the interval; nevertheless, it is not effective for discontinuous or piecewise differential equation systems. Additionally, the separation response is piecewise due to switching between states. Therefore, the dynamic response, based on the wheel–road separation assumption, would be calculated directly by selecting the maximum amplitudes from the time response for each input frequency. A combination of frequency domains for two states, involving no-separation and separation, is illustrated in Figure 9. The solid curves represent the in–contact frequencies in Figure 7, while the dashed curves describe the actual response under the separation assumption. At low input frequencies, the in–contact and no–contact frequencies are completely consistent, but they suddenly deviate around $\omega = 20\,rad/s$, which is referred to as the separation point of the system. After this point, the frequency response seems to be larger than that without the separation assumption. The separation point is the same for the body bounce, roll motion, and displacements of the two tyres. The frequency responses will be analysed in more detail in the forthcoming figures.

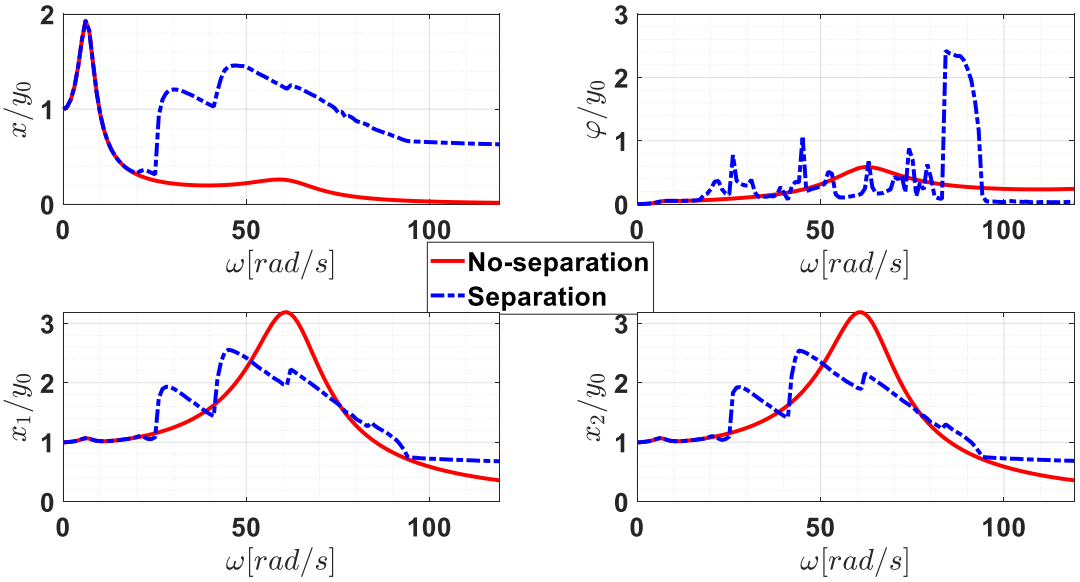

Figure 9. Frequency domain of a half–car system for the no–contact assumption

In a real vehicle, the position of the mass centre is near the middle, so the dynamic responses of the right and left wheels are similar under the same road excitation. It is proven by the subplot in Figure 9. The left wheel's frequency response x_1/y_0 is revealed in Figure 10, highlighting a separation zone. This zone appears when the wheel lifts off from the rough road at the separation point *S,* which is the intersection of the limiting vertical line and the horizontal line of static compression x_{T1}. The separation response is chaotic and generally has a greater amplitude than the in–contact frequency, except around the second resonant frequency; indeed, the actual frequency response with the wheel–road separation assumption should be recalculated. These occurrences of separation could be postponed when the vehicle is designed with a strategy to increase the separation frequency ω.

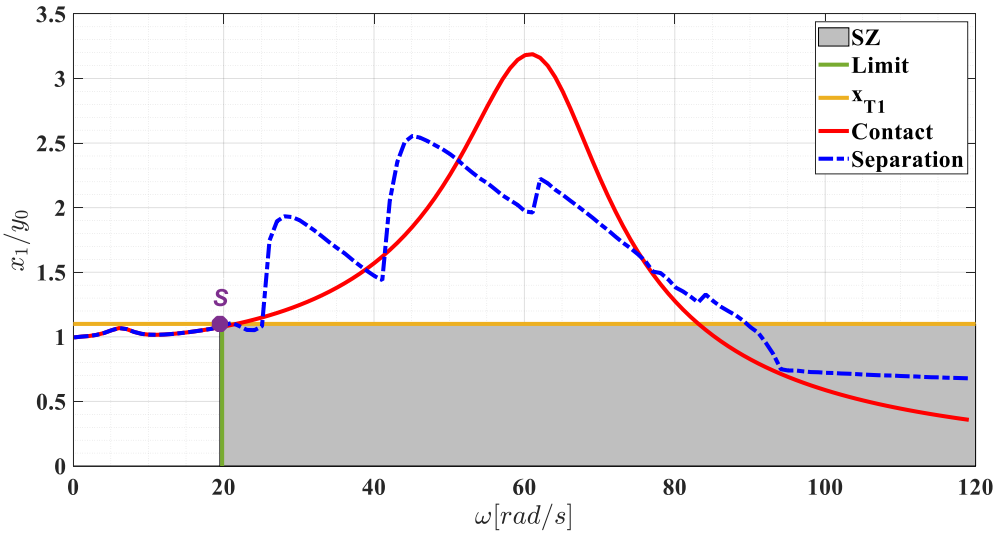

Figure 10. Comparison of frequency domains of the right wheel

The separation process of body bounce is illustrated in Figure 11. This separation point *S* of the body is the same as that of the two tyres as previously analysed, while the actual amplitude of the body bar is significantly higher in the no–

contact zone, as indicated by the dotted curve. In terms of factors influencing passenger comfort, the vibrating response in the body bar plays a vital role, as it directly creates forces on the driver and goods. Thus, the uncomfortable response is significantly increased at high input frequencies where separation phenomena happen. In more detail, the body motion depicts a difference of over six times, even ten times at certain points. The body bounce will directly create a vertical force on the passengers, and ride comfort is evaluated based on the criteria of vertical force; therefore, the frequency domains of the body must be investigated accurately, considering the tyre–road interaction.

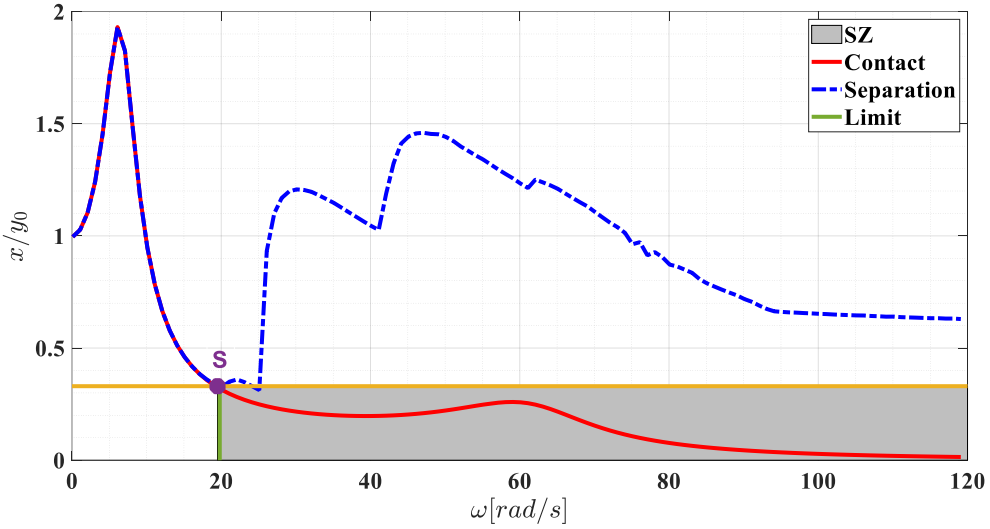

Figure 11. A comparison of the vehicle body's frequency response

The roll angle of a vehicle typically ranges from 2 to 5 degrees when driving on a smooth road under standard conditions [27]. However, during turns or when facing unstable situations, the roll angle may increase, typically not surpassing 7 to 10 degrees in most vehicles [28]. If the roll motion exceeds the limitation, the vehicle becomes unstable and can experience a rollover. Indeed, investigating the roll dynamics is necessary under consideration of tyre–road separation. As displayed in Figure 12, the ratio of the roll angle to the road's amplitude of the half–car depends on the input frequency. The ratio is almost below 1 for both curves, including separation and no-separation, which is equivalent to 0.1 rad (6 degrees) because the value of the road's amplitude, y_0, is 0.1 m. It is noted that the roll motion is extremely high at an input frequency period of ω ranging from 83 to 94 *rad/s*. This area is often referred to as the danger zone, or *DZ*, where a rollover is most likely to occur. This means that a rollover will happen if tyre–road separation is considered.

Roll response is the most uncomfortable vibration in a vehicle. Figure 13 is another attempt at depicting a comparison of roll frequencies for both no–contact and in–contact conditions under low torsional stiffness, $k_R = 1000\ N/m$. Although the separation point S is postponed, at a higher input frequency $\omega = 25\ rad/s$, the roll amplitudes are extremely high, exceeding the rollover limit. Specifically, there are two dangerous zones DZ_1, DZ_2. Comparing these results with those in Figure 12 shows that the half–car system requires a suitable anti–roll bar to reduce roll motion.

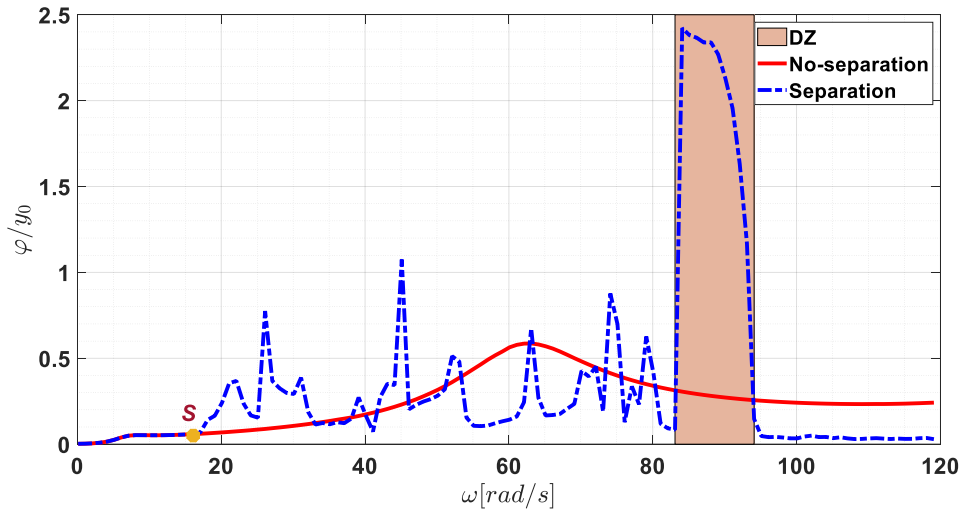

Figure 12. Comparison of frequency domains of roll dynamics

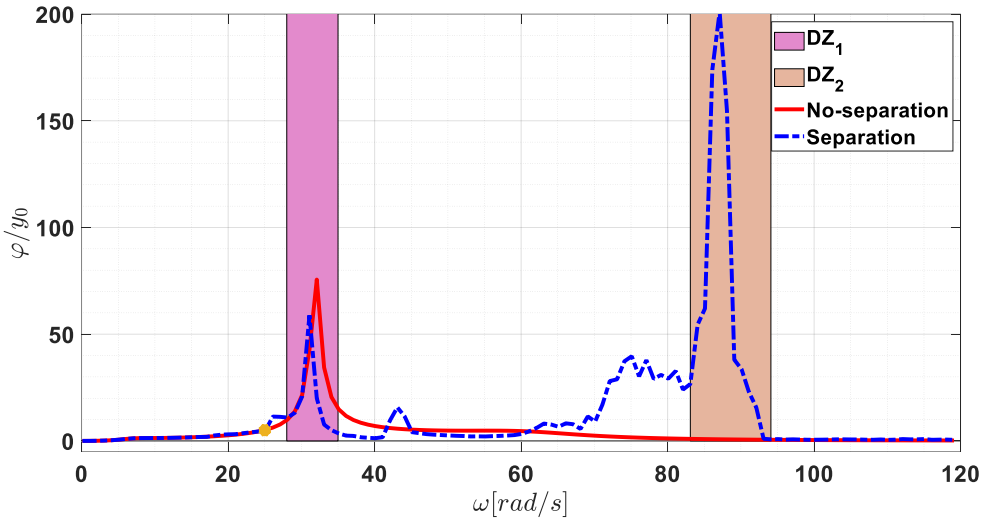

Figure 13. Comparison of the frequency domains of roll dynamics with low anti–roll stiffness

Stability depends on road conditions, velocity, the suspension system, and the vehicle's structure [29–31]. This study focuses on understanding how the mass centre affects its balance. Hence, the vibration dynamics analysis needs to be conducted by shifting the location of the mass centre. In half–car vibrating models, the location of the vehicle's centre is determined by the distances b_1, b_2, and b. To facilitate the examination, those distances are replaced by a position ratio $p = b_1/b$. The body roll angle across a wide range of centre positions is examined in Figure 14, where the series of roll motions has been plotted in four planes. When the vehicle's centre is positioned at the midpoint, with $p = 0.5$, no body roll occurs throughout the investigation period. However, as the centre shifts farther from the middle, the roll response increases significantly.

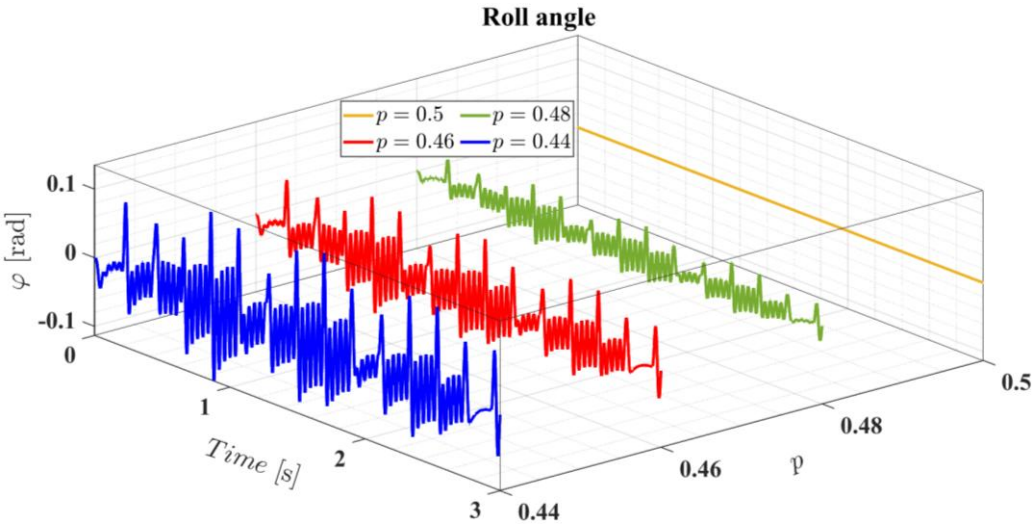

Figure 14. Roll angles following the length ratio

To gain a comprehensive understanding of the roll motion, a frequency domain analysis of the roll needs to be performed over a wide range of mass centre locations, as shown in Figure 15. In a real vehicle, the maximum position ratio, $p = b_1/b$, is 0.5, since beyond this value, the roles of the left and right wheels switch. Additionally, the minimum position ratio can be around 0.4. Indeed, the roll dynamics are investigated based on the location of the mass centre, ranging from 0.3 to 0.5. The most important data appears around 0.5, where points *A*, *B*, *C*, and *D* represent the maximum roll angle obtained from each plane in Figure 14. These points, B, C, and D show that the proposed model is 16% more accurate than the older one. The locus of points representing the maximum angle corresponding to each value of the mass centre's position p forms the separation frequency, as indicated by the dashed curve. Meanwhile, if the assumption of wheel separation is ignored, the frequency characteristic of the roll motion becomes a linear line directly proportional to the position of the mass centre. In conclusion, the angle of roll motion is directly proportional to the centre position ratio. Alternatively, if the separation assumption is ignored, the resulting roll angle is smaller, which is insufficient to predict the danger of rollover, indicating that the proposed method offers greater accuracy. As mentioned in the previous analysis, a large roll angle can cause the vehicle to become unstable and even lead to a rollover. Therefore, this study suggests that to prevent rollover and improve stability, the vehicle's centre of mass should be placed near the middle.

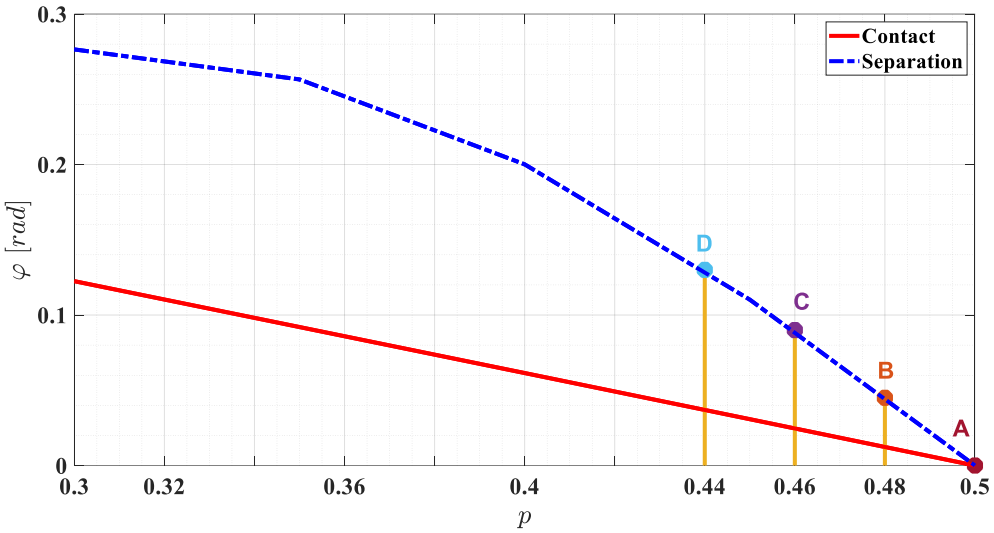

Figure 15. Roll motion in the frequency domain

4. CONCLUSIONS

The wheel–road separation phenomena in the frequency response have been analysed utilising the half–car suspension model. Initially, the time response has been investigated for the in–contact case. The simulation outcomes have been compared to the no–contact scenario, revealing a discrepancy in vibrating amplitude of more than five times after the separation point. Vertical displacements of the vehicle body were analysed over a broad range of road inputs, demonstrating substantial variations at high road amplitudes and frequencies. Based on the vehicle body's frequency, the optimal areas for longitudinal velocity are identified to avoid resonance and enhance ride comfort.

Furthermore, the vibration dynamics have been examined through phase portraits and in the frequency domain. The roll response has also been examined in relation to road excitations and the placement of anti–roll stiffness. The results suggest that the roll angle decreases significantly, making it easier to avoid a dangerous zone when the torsional stiffness is high. Ultimately, it is recommended that a proper anti–roll bar should be structured to improve ride comfort for passengers, and the vehicle's centre of mass should be positioned near the middle to enhance and prevent rollover. In future work, the outcomes could be compared to a half–car rig that includes additional nonlinear characteristics to assess the relevance of the findings when applied to real–world car ride issues.

ACKNOWLEDGEMENTS

The authors do not receive any financial support for the paper.

CONFLICT OF INTEREST

The authors declared that there are no conflicts of interest with any research in the paper.

AUTHORS CONTRIBUTION

Nguyen Dang Quy: Conceptualisation, Investigation, Software, Writing – Original Draft, Visualisation;

Nguyen Truong Sinh: Investigation, Writing – Original Draft, Editing, Visualisation;

Vu Ngoc Tuan: Writing– Reviewing and Editing, Software;

To Viet Thanh: Writing– Reviewing and Editing;

Vu Manh Dung: Formal analysis, Data Curation;

Tran Cong Thuc: Conceptualisation; Writing– Reviewing and Editing;

Pham The Hung: Formal analysis, Resources;

Reza N. Jazar: Methodology, Writing– Reviewing and Editing, Supervision.

REFERENCES

[1] A. E. D. Rabhi, K. Hartani and Y. Guettaf, "Estimation of vehicle tire effective rolling radius and vertical wheel/road contact force," *Proceedings of the Institution of Mechanical Engineers, Part D: Journal of Automobile Engineering*, vol. 239, no. 7. pp. 2982 – 2991, 2025

[2] R. Rajamani, *Vehicle Dynamics and Control*, 2nd Edition, New York: Springer, 2012.

[3] T. D. Gillespie, *Fundamentals of Vehicle Dynamics*, Society of Automotive Engineers, Warrendale, PA, 1992.

[4] M. El-Gindy and Z. El-Sayegh, *Road and Off-Road Vehicle Dynamics*, Cham, Switzerland: Springer, 2023.

[5] Q. D. Nguyen, S. Milani, H. Marzbania, and R. N. Jazar, "Vibration analysis of the bicycle–car model considering tyre–road separation," *SAE International Journal of Commercial Vehicles*, vol. 15, pp. 111-124, 2021.

[6] O. Lukoševičienė and E. Sokolovskij, "Movement of the vehicle being braked when some wheels are incapable of braking or have lost touch with the road surface," *Transport*, vol. 21, no. 1, pp. 8 - 11, 2006.

[7] P. Múčka, "Influence of tyre–road contact model on vehicle vibration response," Vehicle System Dynamics, vol. 53, no. 9, pp. 1227-1246, 2015.

[8] Q. D. Nguyen, S. Milani, H. Marzbani, and R. N. Jazar, "Tyre–road separation time reduction by an adaptive PID controller utilising particle swarm optimisation algorithm," *SAE International Journal of Commercial Vehicles*, vol. 14, no. 4, pp. 37-50, 2021.

[9] Q. D. Nguyen, S. Milani, H. Marzbani, and R. N. Jazar, "Vehicle ride analysis considering tyre–road separation," *Journal of Sound and Vibration*, vol. 521, p. 116674, 2022.

[10] L. Konieczny, P. Fabis, J. Matijošius, K. Duda, P. Deuszkiewicz and A. Kilikevičius, "Analysis of the Impact of Vibrations on the Driver of a Motor Vehicle," *Applied Sciences*, vol. 15, no. 10, art. 5510, 2025.

[11] B. Chen, P. Ding, G. Wei, C. Xiong, F. Wang, J. Yu, et al., "A study on the contact characteristics of tyres–roads based on pressure-sensitive film technology," *Materials*, vol. 16, no. 18, pp. 6323, 2023.

[12] A. Reński, M. Brukalski, H. Sar, M. Abramowski, P. Fundowicz and K. Rokicki, "Determining tyre adhesion characteristics based on road tests of automobiles," *Sensors*, vol. 24, no. 23, art. no. 7447, 2024.

[13] O. Lukoševičienė, M. Bogdevicius, S. Nagurnas and R. Pečeliūnas, "Comparative research of a motor car motion in the case of the loss of contact with the road surface," *Transport*, vol. 19, no. 1, pp. 20-23, 2004.

[14] Q. D. Nguyen, *Tyre–road separation in bicycle–car model*, in *Design Engineering Problems*, New York: Springer, 2024.

[15] Q. D. Nguyen, S. Milani, D. Q. Vo, D. Phan, H. Marzbani, and R. N. Jazar, "The impact of mass ratio on the tyre–road separation in vehicle vibration dynamics," *Proceedings of the Institution of Mechanical Engineers, Part C: Journal of Mechanical Engineering Science*, p. 09544062251349050, 2025.

[16] A. M. C. Odhams and D. Cebon, "An analysis of ride coupling in automobile suspensions," *Proceedings of the Institution of Mechanical Engineers, Part D: Journal of Automobile Engineering*, vol. 220, no. 8, pp. 1041–1061, 2006.

[17] J. Marzbanrad, P. Poozesh, and M. Damroodi, "Improving vehicle ride comfort using an active and semi–active controller in a half–car model," *Journal of Vibration and Control*, vol. 19, no. 9, pp. 1357–1377, 2013.

[18] P. Gandhi, S. Adarsh, and K. I. Ramachandran, "Performance analysis of half–car suspension model with 4 DOF using PID, LQR, Fuzzy and ANFIS controllers," *Procedia Computer Science*, vol. 115, pp. 2–13, 2017.

[19] B. C. Hamblin, R. D. Martini, J. T. Cameron, and S. N. Brennan, "Low–order modelling of vehicle roll dynamics," *2006 American Control Conference*, pp. 8, 2006.

[20] A. Chokor, R. Talj, M. Doumiati, and A. Charara, "Effect of roll motion control on vehicle lateral stability and rollover avoidance," *2020 American Control Conference (ACC)*, pp. 4868–4875, 2020.

[21] A. A. Ferhath and K. Kasi, "Dynamic modelling of a semi–active suspension system for a half–car role model utilising PID control techniques," *Multiscale and Multidisciplinary Modelling, Experiments and Design*, vol. 8, no. 131, 2025.

[22] I. Iben Ammar, M. Doumiati, R. Talj, A. Chokor, and M. Machmoum, "Analysis and control of the vehicle roll dynamics using sum of squares polynomial approach," *Journal of Systems Science and Complexity*, vol. 37, no. 6, pp. 2318-2346, 2024.

[23] R. C. Dorf and R. H. Bishop, *Modern Control Systems*, 14th ed., Pearson, New York, 2021.

[24] J. Y. Wong, *Theory of Ground Vehicles*, 5th ed., Hoboken, NJ: John Wiley & Sons, 2022.

[25] Q. D. Nguyen, T. Van Nguyen, D. Q. Vo, T. N. Vu, S. Milani, H. Marzbani, et al., "Vibration analysis of tyre–road separation in a bicycle–car model," *Nonlinear Approaches in Engineering Applications: Automotive Engineering Problems*, pp. 133–162, 2024.

[26] H. Hu, *Vibration Mechanics: A Research-Oriented Tutorial*, Singapore: Springer Nature, 2023.

[27] B. Wiegand, "Mass properties and automotive lateral acceleration," in *10th International Conference on Mass Properties*, Houston, USA, 2011.

[28] K. Parczewski and H. Wnęk, "The influence of vehicle body roll angle on the motion stability and manoeuvrability of the vehicle," *Combustion Engines*, vol. 56, no. 1, pp. 133–139, 2017.

[29] V. Lukoševičius, R. Makaras, A. Rutka, R. Keršys, A. Dargužis, and R. Skvireckas, "Investigation of vehicle stability with consideration of suspension performance," *Applied Sciences*, vol. 11, no. 20, p. 9778, 2021.

[30] T. A. Nguyen, "Assessing the dependence of vehicle rollover on many factors based on new 4D graphs," *PLoS ONE*, vol. 18, no. 4, p. e0284018, 2023.

[31] S. Misaghi, C. Tirado, S. Nazarian, and C. Carrasco, "Impact of pavement roughness and suspension systems on vehicle dynamic loads on flexible pavements," *Transportation Engineering*, vol. 3, p. 100045, 2021.

DEFINITIONS/ABBREVIATIONS

Description	Symbol [Unit]
Body mass	m [kg]
Left, right mass	m_1, m_2 [kg]
Distance	b_1, b_2 [m]
Spring stiffness	k[N/m]
Left, right tyre stiffness	k_{t1}, k_{t2} [N/m]
Left, right damper	c_1, c_2 [Ns/m]
Excitation frequency	ω [rad/s]
Mass moment	I_x [kgm^2]
Mass centre	C
Anti-roll bar stiffness	k_R [N/m]
Period of time	T [s]
Velocity of the vehicle	v [m/s]
Road amplitude	y_0 [m]
Road excitation	x_{r1}, x_{r2} [m]
Vertical body displacement	x [m]
Indicator	I_1, I_2
Acceleration of gravity	g [m/s^2]
Front, rear displacement	x_1 , x_2 [m]
Roll motion	φ
Time	t [s]